microbiology research

MDPI

Article

Predictive Modeling of UV-C Inactivation of Microorganisms in Glass, Titanium, and Polyether Ether Ketone

Amira Chroudi [1,2], Talita Nicolau [2], Narayan Sahoo [3,4], Óscar Carvalho [3,4], Andrea Zille [2], Samir Hamza [1] and Jorge Padrão [2,*]

[1] National Institute of Applied Sciences and Technology, UR17ES22, University of Cartage, Tunis 1080, Tunisia; amira.chroudi@fst.utm.tn (A.C.); samir.hamza@insat.ucar.tn (S.H.)
[2] Centre for Textile Science and Technology (2C2T), University of Minho, 4800-058 Guimarães, Portugal; talitanicolau@2c2t.uminho.pt (T.N.); azille@2c2t.uminho.pt (A.Z.)
[3] Center for Micro Electro Mechanical Systems (CMEMS), University of Minho, 4800-058 Guimarães, Portugal; b8988@dei.uminho.pt (N.S.); oscar.carvalho@dem.uminho.pt (Ó.C.)
[4] Associate Laboratory in Biotechnology and Bioengineering and Microelectromechanical Systems (LABBELS), 4800-058 Guimarães, Portugal
* Correspondence: padraoj@2c2t.uminho.pt; Tel.: +351-253-510289; Fax: +351-253-510293

Abstract: Biomaterials consist of both natural and synthetic components, such as polymers, tissues, living cells, metals, and ceramics. Their purpose is focused on repairing or replacing malfunctioning living tissues and organs. Therefore, it is imperative to ensure the safety and sterility of biomaterials before any contact with living tissue. Ultraviolet (UV)-C irradiation for biomaterial disinfection has been considered due to the high recurrence rate of bacterial infections and to prevent resistance. Physical composition and surface properties and UV-C sensitivity of microorganisms can alter its efficacy. The main objective of this study was to evaluate the efficacy of UV-C in terms of microbial lethality and additional underlying factors contributing to its performance, namely the surface properties. For this purpose, twelve different strains were first screened, from which four microorganism species known to have the ability to cause nosocomial infections were further tested, namely *Escherichia coli*, *Pseudomonas aeruginosa*, *Candida albicans*, and *Candida glabrata*. These microorganisms were inoculated onto slides and disks of various bio contact surfaces, including glass (GLS), titanium (Ti), and poly ether etherketone (PEEK), and exposed to UV-C. The results demonstrate that bacterial pathogens on biomaterial surfaces respond differently to UV-C light exposure, and the bactericidal effect decreased in this order: glass, PEEK, and Ti (0.5 to 2.0 log reduction differences). *P. aeruginosa* ATCC 27853 on glass surfaces was reduced to an undetectable level after being exposed to 6.31 $J.cm^{-2}$ of UV-C, displaying the highest reduction rate observed among all the tested microorganisms, 2.90 $J^{-1}.cm^{-3}$, compared to Ti and PEEK. Similarly, a higher reduction in *C. glabrata* ATCC 2001 was observed on glass; the modeled inhibition displayed a rate of 1.30 $J^{-1}.cm^{-3}$, the highest observed rate among yeast, compared to Ti and PEEK, displaying rates of 0.10 $J^{-1}.cm^{-3}$ and 0.04 $J^{-1}.cm^{-3}$, respectively. The inactivation rates were higher for less hydrophobic materials with smoother surfaces as compared to biomaterials with rougher surfaces.

Keywords: disinfection; indwelling materials; ultraviolet C; bacteria; fungi

Citation: Chroudi, A.; Nicolau, T.; Sahoo, N.; Carvalho, Ó.; Zille, A.; Hamza, S.; Padrão, J. Predictive Modeling of UV-C Inactivation of Microorganisms in Glass, Titanium, and Polyether Ether Ketone. *Microbiol. Res.* **2024**, *15*, 1189–1207. https://doi.org/10.3390/microbiolres15030080

Academic Editor: Luca Grispoldi

Received: 17 May 2024
Revised: 21 June 2024
Accepted: 27 June 2024
Published: 5 July 2024

1. Introduction

Implant device-associated infections are a typical set of complications which have an impact on the prognosis of orthopedic surgery. Infections caused by bacteria or biofilms may result in implant failure and patient death [1]. According to the statistics, it is estimated that implant-related bacterial infections cause more than 100,000 deaths per year in America [2]. According to the scientific literature, prosthetic infection occurs in about 1% of all total joint replacements. However, this percentage rises dramatically in

the case of revision surgery [3]. Moreover, this number increases up to 10-fold after a device has been replaced or upgraded. Implant infections may be divided into two major groups according to the period during which the infection unfolds after the surgery: within one month or after 12 months [4]. Infections can be categorized according to the time interval between surgery and the onset of clinical symptoms. Early infections are primarily attributed to highly pathogenic microorganisms, such as *Staphylococcus aureus*, and occur within three weeks of implanting an orthopedic device. Delayed infections, on the other hand, are commonly caused by less virulent bacteria like coagulase-negative *Staphylococci*, and they develop between three and ten weeks after. Ultimately, late infections occur after more than ten weeks after implantation and are caused by either hematogenous seeding or the recurrence of an inadequately treated early infection [5]. Medical implant-related infections evade immune protection mechanisms and are challenging to tackle using antimicrobial products due to the fact the organisms are enclosed inside a protected microenvironment, hampering the prevention and treatment of established bacterial-associated infections, and often persist until the implant is removed, which is the standard treatment. Implant infections show considerable resistance to antibiotics and host defenses and often persist until the implant is removed. Biofilm infection is a leading cause of failure in biomaterial implants [6]. Microorganisms have a notable ability to attach to biomaterial surfaces and form multicellular structures known as biofilms, which can potentially affect the safe use and function of both tissues and implanted clinical gadgets, and are accountable for about 60–70% of nosocomial infections, especially in seriously ill patients [7]. These biofilms represent communities of complex microorganisms, which are typically attached to a surface and embedded into a 3D extracellular matrix. The biofilm development process consists of five distinct stages. In the first stage, cells adhere to the surface and produce extracellular polysaccharide, which leads to the formation of the biofilm. During the formation of the biofilm, there are numerous elements that are chargeable for the preliminary adhesion of the microbes, along with polarity, London–van der Waals forces, and hydrophobic interactions. There are numerous bacteria adhered to the protein floor contributing to the preliminary adhesion and ensuing biofilm formation. The biofilm includes proteins, electrolytes, and a few unidentified molecules. A polysaccharide structure known as capsular polysaccharide/adhesion (PS/A) leads to the initial adhesion and slime production. The adherence of the bacteria to the inert surface leads to the formation of a stable microcolony. Bacterial cell proliferation and intercellular adhesion take place once the microbes have adhered to the surface of the implants. During this accumulation phase, the microbes multiply and form numerous layered molecular clusters at the implant surface. Extra-polymeric substances (EPSs) are produced in this phase, which are responsible for enhancing cell binding and adhesion to the surface [8,9]. The EPS matrix acts as a barrier and protects the microbes during adverse conditions. Thus, a contaminated implant can be a reservoir for infection of the surrounding tissue, where bacteria can reside intracellularly. Biomedical device-associated infections are resistant to immune defense mechanisms and are difficult to treat with antimicrobial agents due to the protected microenvironment maintained within the EPS, hampering treatment. The biofilm matrix provides protection to the embedded bacterial cells by preventing the penetration of certain antibiotics and host immune cells. Nevertheless, tissue damage caused by surgery and foreign body implantation further increases the susceptibility to infections, activates host defenses, and stimulates the generation of inflammatory mediators; these are enhanced by bacterial and fungal activity. Commonly, implant infections may arise primarily from the host's skin and from medical staff during implant insertion [10–12]. Subsequently, bacteria migrate through incision channels to the device surfaces in the host and through hematogenous spreading. The microbiological profile is relevant to implant-linked infections. The type and location of infection depend on the biomaterial type and location [13–16]. Gastrointestinal and urological implants can be colonized by diverse strains. The primary contaminants in urological implants are *S.*

aureus and *Escherichia coli*. Meanwhile, the most frequent cause of infection in gastrointestinal implants is the pan-antibiotic-resistant *Acinetobacter baumannii*, a bacterium resistant to desiccation and nutrient deficiency and which forms a stable biofilm resistant to several antimicrobials. Thus, *A. baumannii* is presently among the leading microbes targeted for the development of new antibiotics [13]. ◎ pportunistic *Staphylococci*, *Enterococci*, *Enterobacteriaceae*, and *Candida* infections are commonly found at sites such as blood vessel catheters, dental implants, cerebrospinal fluid shunts, peritoneal dialysis catheter (CAPD) arterial grafts, cardiac and total joint replacements (endoprostheses), and ocular and neuro-implants [17]. The most common biofilm-forming pathogens found on these medical devices are *E. coli*, *Pseudomonas aeruginosa*, *Staphylococcus epidermidis*, *S. aureus*, *Candida albicans*, and *Candida tropicalis* [18]. Among the pool of pathogenic microorganisms, methicillin-resistant aureus (MRSA) and *E. coli* are the major causative agents of medical implant infections, particularly in immunocompromised patients, namely who have cancer, acquired immunodeficiency syndrome (AIDS), or an autoimmune disease. These cases are prone to facilitating implant-related systemic infections, being the main causes of mortality [18,19]. Evaluation reports suggest that the prevalence of pathogens in patients with stent-associated respiratory infection includes 50% *S. aureus*, 35.7% *P. aeruginosa*, and 14.3% *C. albicans* [19]. For cardiac implants, such as permanent pacemakers and defibrillators, the most frequent pathogens involved include methicillin-resistant MRSA, *Pseudomonas* spp., *E. coli*, and *S. epidermidis* [19–21]. The bacteria/surface material interface is a complex topic, involving the chemical and physical–chemical characteristics of both the material surface and the bacterial cell wall, as well as the biological characteristics of the bacteria [21]. Furthermore, proteins and other biomolecules coming from the surrounding medium influence the bacteria/material interface by adsorbing onto the material surface prior to any adhesion of the bacteria [21]. In this case, implants, as surgical components that have intimate contact with bone, need to be properly sterilized prior to implantation or during storage [22,23]. Therefore, developing biomaterials able to favor cell adhesion without also promoting bacterial adhesion appears to still be a challenge. As an alternative to chemical disinfectants, ultraviolet lights have been investigated for their ability to inactivate pathogens [23,24]. UV radiation is a prevalent method for sterilizing the surfaces of materials and biopolymer implants. UV-C disinfection outperforms hydrogen peroxide disinfection, as well as other chemical-based disinfectants, including chlorine and chloramine. However, chemical sterilization is one of the main causes of corrosion in medical implants, which is one of the factors responsible for a loss of cutting efficiency [25]. Since UV irradiation is not ionizing, it can be used to sterilize high-risk materials [26]. The penetration of UV-C light into substrates is limited, and optical technology may be employed to extend this limit. A study by Vezeau et al. explored the effects of sterilization on titanium surface characteristics and fibroblast attachment in vitro. They reported that titanium surface characteristics can be altered by steam autoclave sterilization. Furthermore, this sterilization process diminished murine fibroblast attachment when compared to UV-C irradiation sterilization [8]. UV radiation is electromagnetic, with its wavelengths shorter than visible light. The electromagnetic spectrum comprises energies with both electrical and magnetic properties that can be categorized based on wavelength and photonic interactions with substances. The UV wavelengths range between high-energy X-rays (<100 nm) and the lower-energy visual spectrum (>400 nm) [9]. Ionization with a change in the atomic charge of matter results from the interactions between the energy and the substances under a wavelength of less than 100 nm. UV irradiation is divided into four distinct spectral areas according to wavelength, namely vacuum UV (100–200 nm), the most energetic wavelength range, which interacts with oxygen atoms and organic molecules at low doses; UV-C (200–280 nm); UV-B (280–315 nm); and UV-A (315–400 nm), such that UVC is found to be the most effective, especially for biopolymers since UV-C can be directly applied to acute medical implant infections to kill pathogens without unacceptable damage to host tissue [9,27,28]. Moreover, UV-C inactivates

microbes through damaging their genetic material [10]. The UV-C spectrum, in particular the 250–270 nm range, is strongly absorbed by microbial nucleic acids, which is commonly stated to reach its maximum at 262 nm [13]. Sterilization by UV-C can be optimized based on the wavelength and the duration of exposure [5,29,30]. The purpose of this study is to evaluate the effects of UV-C for inactivating bacteria of three different experimentally contaminated surfaces commonly found in implanted medical devices, namely glass (GLS), titanium (Ti), and poly ether etherketone (PEEK).

2. Materials and Methods

2.1. Sample Preparation

The efficacy of UV-C exposure on GLS was evaluated using pre-cleaned glass slides measuring 22 × 22 mm (Menzel-Gläser, Braunschweig, Germany) and with a standard thickness of 0.95 to 1.05 mm. Disk-shaped Ti6A14V titanium samples (8.0 mm diameter, 1.7 mm thickness) were prepared by machining commercially available pure titanium (US, ASTM B 348, Grade V) from VSMP® TIRUS. The PEEK disks used in this research were of a uniform size and thickness (8 mm in diameter and 2 mm thick) and came from Dental Direkt GmbH (DD peek MED, D-32139 Spenge, Germany). Prior to UV-C irradiation, all the samples were immersed for 15 min in a 70% (*v*/*v*) ethanol solution and rinsed with deionized water. Afterwards, they were air-dried inside a biological safety cabinet (Class II, Type A2) [31]. These samples were then placed into a sterile Petri dish using sterile tweezers and inoculated. Subsequently, the samples were exposed to UV-C irradiation.

2.2. UV-C Treatment

A 75 W UV-C germicidal lamp (UV-C 254 nm) was used. The UV experimental setup is displayed in Figure 1. The samples were placed in a 60 mm Φ Petri dish (without a lid) on top of a sample holder at a fixed distance of 25 cm from the UV-C lamp. Immediately adjacent to the sample holder, a UV-C probe recorded the irradiance, using the radiometer HD 2102.2 (Delta ® HM, Padua, Italy) equipped with a UV-C probe (LP471UVC, Delta ® HM, Padua, Italy). The UV-C lamp was turned on and off using a remote-controlled power socket.

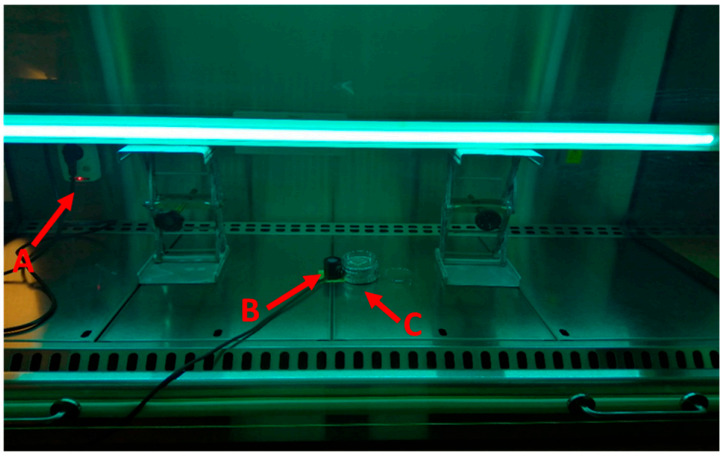

Figure 1. Experimental setup: A—remote controlled power socket; B—UV-C probe; C—sample holder.

The samples and the probe were positioned beneath the center of the lamp. The UV-C dose was estimated according to Equation (1) [32]:

$$Q(t) = \sum_0^t u(t) \times \Delta t\,,\ \Delta t = 1\ s \quad (1)$$

where u(t) corresponds to the instantaneous value of UV-C irradiance compared with time t. The UV-C lamp was heated for at least 10 min before each test.

2.3. Temperature Variation during Irradiation

The UV-C treatments were performed at room temperature, which was approximately 22 °C. Nevertheless, to exclude the influence of temperature during the UV-C treatment, the temperature at the sample holder position was monitored using an alcohol thermometer after 5, 15, 30, and 60 min. To enhance the temperature variation resolution, ImageJ (1.54 g, National Institutes of Health, Bethesda, MD, USA) software was used [33]. Furthermore, to analyze the temperature variation for GLS, Ti, and PEEK, their temperature when exposed to UV-C was monitored using a thermographic camera (testo 876, Titisee-Neustadt, Germany) and recorded at 5, 15, 30, 45, and 60 min.

2.4. Absorbance and Reflectance

The absorbance and reflectance of GLS, Ti, and PEEK were analyzed in a UV–visible light spectrometer Shimadzu UV-2600 (Kyoto, Japan), using a wavelength range between 200 and 800 nm and a resolution of 1 nm.

2.5. Microorganisms

The bacteria used in this study were acquired from the American Type Culture Collection (ATCC): Escherichia coli ATCC 25922, Escherichia coli ATCC 15597, Escherichia coli ATCC 8739, Staphylococcus aureus ATCC 6538, Staphylococcus epidermidis ATCC 35984, Pseudomonas aeruginosa ATCC 27853, and Acinetobacter baumannii ATCC 19606. Candida albicans ATCC 10231, Candida krusei ATCC 10231, Candida glabrata ATCC 2001, Candida parapsilosis ATCC 90018, and Candida tropicalis ATCC 13803 were the fungi used in this investigation. The liquid and solid culture media used for all the experiments were tryptic soy broth (TSB) and tryptic soy agar (TSA). The culture conditions comprised a shaking speed of 120 rpm and temperatures of 37 °C for bacteria and 30 °C for fungi. Pre-inocula were prepared from a single colony collected from a previously prepared culture in TSA. Bacteria and fungi pre-inocula were incubated for approximately 12 h and 36 h. The pre-inocula concentration was adjusted to 1×10^7 $CFU.mL^{-1}$ in phosphate-buffered saline solution (PBS) (7.4 pH). The antimicrobial efficacy was tested through an adaptation of the standard AATCC 100 TM100 [32,34]. In brief, 5 µL of a microbial suspension with 1×10^7 CFU.mL-1 was placed on the surface of a sample. Then, the samples were irradiated with UV-C (except for the control samples). Subsequently, the samples were immersed in 5 mL of PBS solution and vigorously vortexed for at least 60 s. Afterwards, serial dilutions were performed in PBS and they were inoculated into Petri dishes containing TSA. The Petri dishes were then incubated for 20 h and 48 h, for bacteria and fungi, respectively. The CFUs were then counted, and the viable microorganism concentration was estimated. The reduction in microorganism viability was determined according to Equation (2):

$$\text{Log reduction } (CFU.mL^{-1}) = \text{Log } [\text{Control } (CFU.mL^{-1})] - \text{Log } [\text{UV-C exposed } (CFU.mL^{-1})] \quad (2)$$

where Control corresponds to the microorganism concentration inoculated into the sample without UV-C exposure, and UV-C exposed represents the microorganism concentration inoculated into the sample subjected to UV-C exposure. Qualitative classification of the reduction was reported according to the description presented by Vieira and colleagues [34]. All the experiments were plated in duplicate and replicated three times.

2.6. Reduction Models

The collected data correlating the concentration reduction in the microorganisms were modeled using an exponential equation, the Monod equation, the Michaelis–Menten

equation, and a logistic equation (Supplementary Tables S2–S4). The model with a coefficient of determination (r^2) closer to unity was the determinant factor for electing a specific model. The logistic equation (Equation (3)) displayed the highest fit values.

$$R(t) = \frac{R_{max}}{1 + e^{-\mu(R_{max} - x_{min})}} \quad (3)$$

where R(t) corresponds to the concentration reduction at dosage (t), R_{max} the maximum reduction, R_{min} the minimum reduction, and μ the rate of reduction.

3. Results and Discussion

3.1. UV-C Efficacy on GLS

The recorded temperature variation is exhibited in Figure 2.

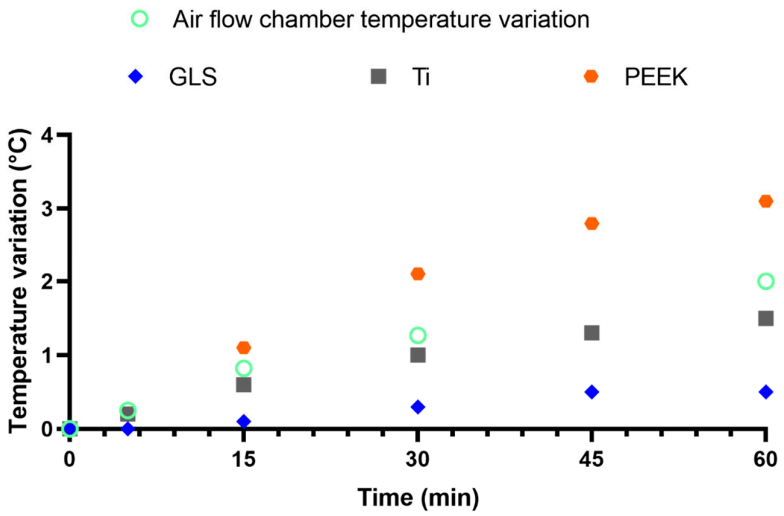

Figure 2. Temperature variation within the air flow chamber (thermometer), GLS, Ti, and PEEK (thermographic camera) during UV-C exposure.

The temperature increase ratio followed a nearly linear increase (Supplementary Table S1). The air flow chamber increased by approximately 0.04 °C.min^{-1}. The temperature variation of the tested materials was marked at 0.01, 0.03 and 0.06 °C.min^{-1} for GLS, Ti, and PEEK, respectively. The maximum exposure time was 1.5 min; thus, the predicted temperature increase was 0.01, 0.04, and 0.08 °C for GLS, Ti, and PEEK, respectively. The expected temperature increase is far from the optimal temperature for the tested microorganisms, which ranged between 30 and 37 °C. Therefore, temperature was not considered as factor that interfered with the microorganisms' viability. However, it should be noted that PEEK exhibited a 1.5-fold higher rate than the environmental temperature. Meanwhile, GLS exhibited a nearly 4-fold lower temperature increase rate in comparison to the ambient temperature increase.

The UV-C absorbance and reflectance spectra of GLS are displayed in Figure 3.

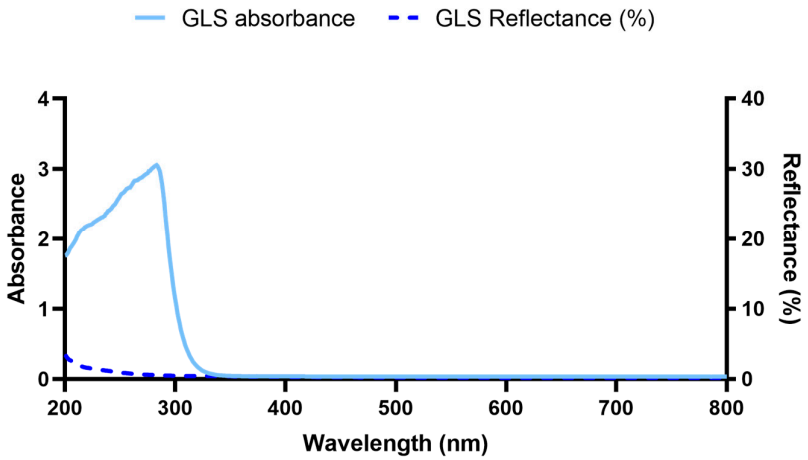

Figure 3. GLS absorbance and reflectance spectra.

From 800 nm to 327 nm (UV-A), it is clear the minimal absorbance of GLS subsequently it sharply increased, reaching its maximum at 283 nm (UV-B). At 254 nm, the maximum irradiation provided by the low-pressure mercury lamp used, the absorbance is considerable [35]. The reflectance at 254 nm is solely 1.0%. Overall, the maximum recorded reflectance was nearly 3.4%. Thus, the reflectance may be considered negligible, with nearly all the UV-B and UV-C irradiation being absorbed by GLS. This is in accordance with the literature, which confirms the opaque nature of GLS below near-UV-B irradiation wavelengths. Only at lower wavelengths do photons possess the required energy to excite silica (the main GLS material) across the band gap, leading to its absorption [36]. These results corroborate the lower temperature increase by GLS in comparison to Ti and PEEK.

The microorganisms were irradiated with the UV-C doses summarized in Table 1.

Table 1. Different UV-C dosages applied to the samples inoculated with the distinct microorganisms.

UV-C (J.cm^{-2})
3.83
6.31
12.82
19.20
25.55
38.34
44.66
57.79
75.68

The results obtained for the GLS slides are described in Figure 3. Table 2 encompasses the modeled reduction parameters. Interestingly, of the three strains of *E. coli* tested, *E. coli* ATCC 25922 and *E. coli* ATCC 8739 exhibited a similar profile. Irradiation of 6.31 J cm^{-2} resulted in the absence of colony counts. However, *E. coli* ATCC 15597 exhibited distinct behavior. The required irradiation to obtain an undetectable level of viable bacteria was 12.82 J.cm^{-2} (Figure 4A). The rate of inhibition of these bacteria was also different among the three *E. coli*. The highest reduction ratio was observed for *E. coli* ATCC 8739. This ratio was nearly 1.5-fold lower for *E. coli* ATCC 25922 and was approximately 5-fold lower for *E. coli* ATCC 15597 (Table 2). *P. aeruginosa* ATCC 27853 and *A. baumannii* ATCC 19606

exhibited a highly similar reduction profile. When exposed to 6.31 J.cm^{-2} of UV-C, no viable bacteria were detected (Figure 4B). The rate of reduction was just slightly lower for *A. baumannii* in comparison to *P. aeruginosa* (0.8-fold lower). In addition, their reduction rates are within the same range as that for *E. coli* ATCC 25922. And *S. epidermidis* ATCC 35984 was reduced to an undetectable level after being exposed to 3.83 J.cm^{-2} of UV-C, displaying the highest reduction rate observed among all the tested microorganisms, at 4.20 J^{-1}.cm^{-3} (Figure 4C). *S. aureus* ATCC 6538's detectable viability was observed after 12.82 J.cm^{-3}. Furthermore, *S. aureus*'s reduction rate was within the ranges observed for *E. coli* ATCC 25922, *P. aeruginosa*, and *A. baumannii*. UV-C irradiation of the yeasts inoculated into GLS displayed distinct inhibition profiles. At 19.17 J.cm^{-2}, *C. glabrata* was the yeast that exhibited the highest susceptibility to UV-C irradiation (Figure 4F). At 19.20 J.cm^{-3}, no viable *C. glabrata* were detected. The modeled inhibition displayed a rate of 1.3 J^{-1}.cm^{-3}, the highest observed rate among the yeasts. After irradiation of 44.66 J.cm^{-3} of UV-C, no viable colonies of *C. albicans*, *C. krusei*, *C. parapsilosis*, or *C. tropicalis* were detected (Figure 4D–H).

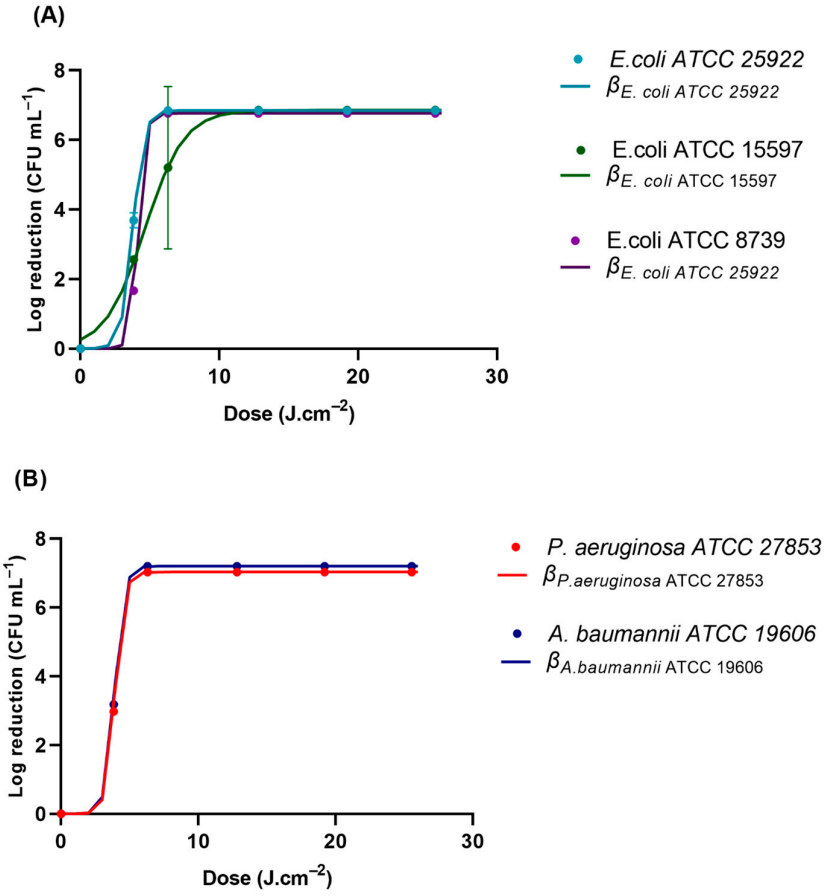

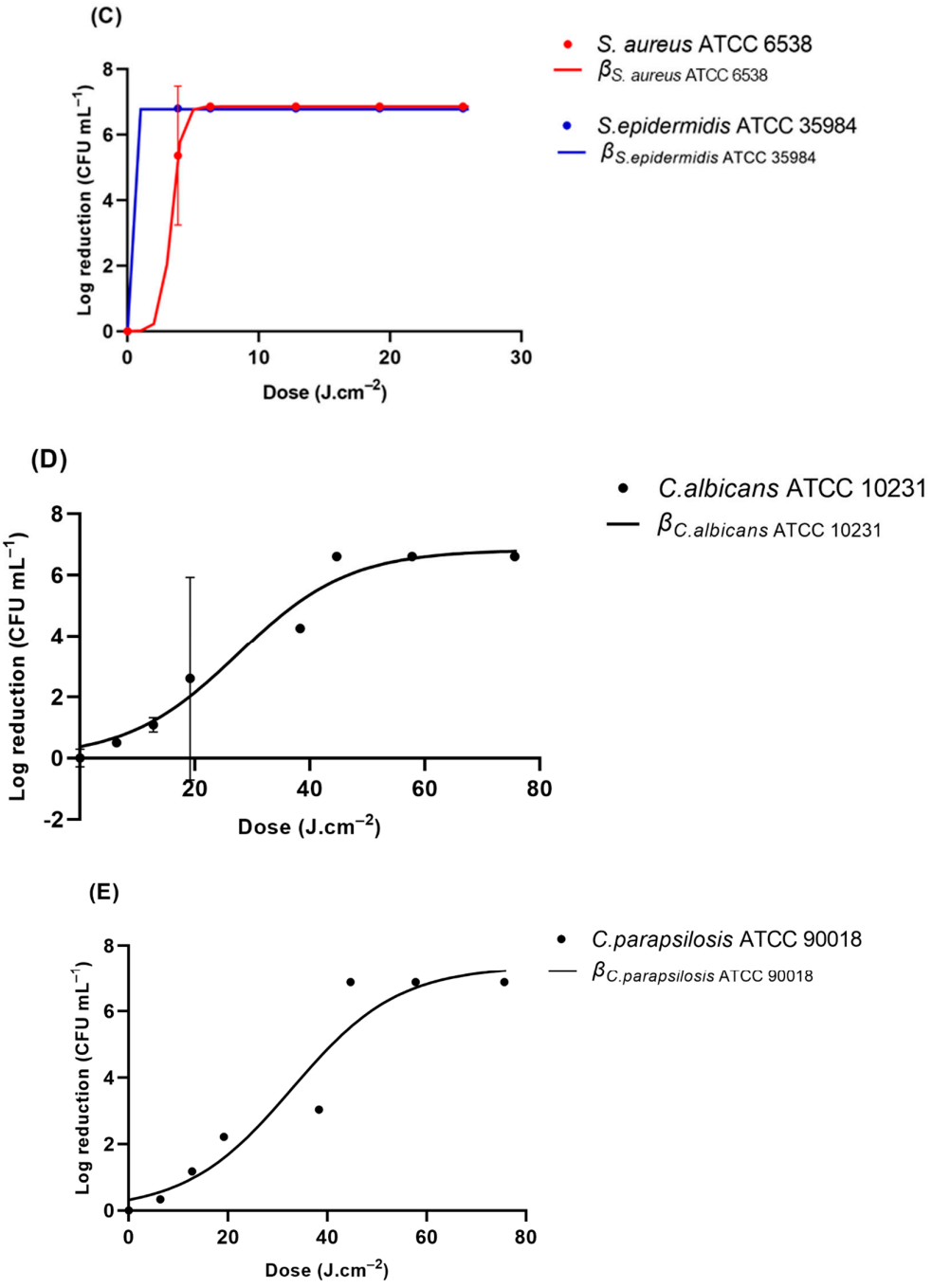
(C)
Log reduction (CFU mL^{-1})
Dose (J.cm^{-2})
S. aureus ATCC 6538
$\beta_{S.\ aureus\ ATCC\ 6538}$
S.epidermidis ATCC 35984
$\beta_{S.epidermidis\ ATCC\ 35984}$
(D)
Log reduction (CFU mL^{-1})
Dose (J.cm^{-2})
C.albicans ATCC 10231
$\beta_{C.albicans\ ATCC\ 10231}$
(E)
Log reduction (CFU mL^{-1})
Dose (J.cm^{-2})
C.parapsilosis ATCC 90018
$\beta_{C.parapsilosis\ ATCC\ 90018}$

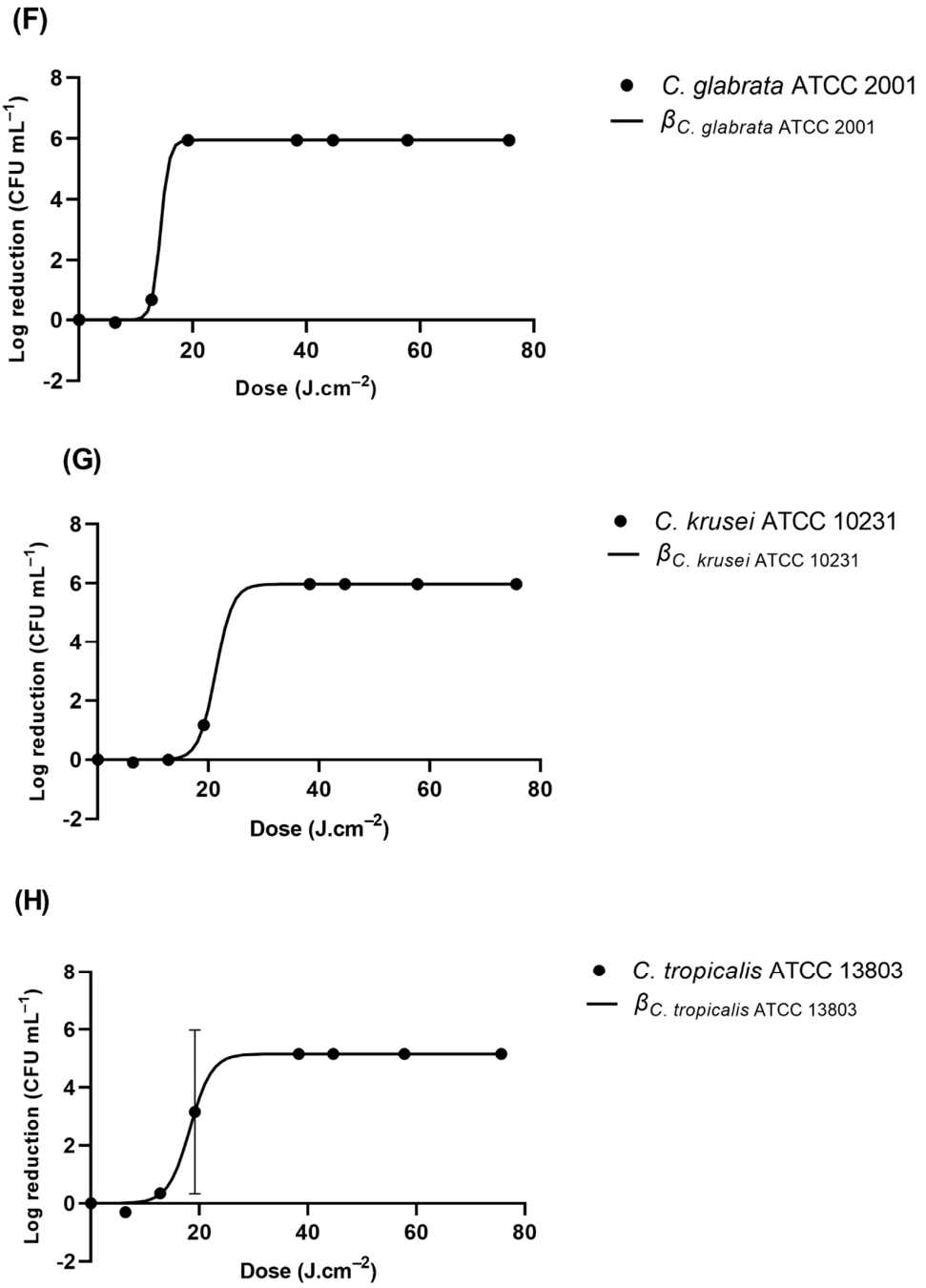

Figure 4. Viability reduction profiles of (**A**) *E. coli* strains ATCC 2522, ATCC 15597, and ATCC 8739, (**B**) *P. aeruginosa* ATCC 27853 and *A. baumannii* ATCC 19606, (**C**) *S. aureus* ATCC 6538 and *S. epidermidis* ATCC 35984, (**D**) *C. albicans* ATCC 1023, (**E**) *C. parapsilosis* ATCC 90018, (**F**) *C. glabrata* ATCC 2001, (**G**), *C. krusei* ATCC 10231, and (**H**) *C. tropicalis* ATCC 13803 on GLS after UV-C irradiation. β represents the modeled reduction using the logistic equation (Equation (3)).

Table 2 shows that most of the Gram-negative and Gram-positive bacteria were inactivated with a UV-C dose loading of less than 12.82 J cm-3, while the yeasts appeared to be more resistant to the UV-C-induced damage. The inactivation efficacy of UV-C against bacteria differs, which may technically depend on the UV-C fluence required to decrease the number of bacteria by an order of logarithmic magnitude.

Table 2. Microorganism models of inhibition according to UV-C irradiation.

Microorganisms	ATCC Strain	Material	R_{max} (CFU.mL^{-1})	R_{min} (CFU.mL^{-1})	μ (J^{-1}.cm^{-3})	Model	r^2
E. coli	25922	GLS	6.85	6.00×10^{-4}	2.44	Logistic equation	0.9999
E. coli	8739	GLS	6.77	1.95×10^{-6}	3.63	Logistic equation	0.9999
E. coli	15597	GLS	6.86	0.26	0.70	Logistic equation	0.9995
A. baumannii	19606	GLS	7.20	1.00×10^{-4}	2.84	Logistic equation	0.9999
P. aeruginosa	27853	GLS	7.03	6.41×10^{-5}	2.94	Logistic equation	1.0000
S. epidermidis	35984	GLS	6.78	1.00×10^{-2}	4.20	Logistic equation	1.0000
S. aureus	6538	GLS	6.86	1.30×10^{-2}	2.55	Logistic equation	1.0000
C. albicans	10231	GLS	6.83	0.37	0.11	Logistic equation	0.9832
C. glabrata	2001	GLS	5.95	4.03×10^{-8}	1.31	Logistic equation	0.9999
C. tropicalis	13803	GLS	5.165	5.00×10^{-4}	0.50	Logistic equation	0.9991
C. parapsilosis	90018	GLS	7.36	0.32	0.09	Logistic equation	0.9599
C. krusei	2159	GLS	5.97	4.86×10^{-6}	0.66	Logistic equation	0.9999

UV-C is widely known for its antimicrobial activity, which may be attributed to two factors: UV-C's direct activity and reactive species (R◎ S) generation. UV-C photons are absorbed by the pyrimidine (cytosine, thymine, and uracil) and purine (adenine and guanine) nucleic acid residues ubiquitously present in genomic material [37,38]. UV-C photons lead to photoproduct generation after the excitation of these elements into singlet and triplet electronic states [37]. These photoproducts encompass cyclobutane pyrimidine dimers (CPDs) and pyrimidine 6-4 pyrimidone photoproducts (6-4PPs) [39]. Dewar lesions have been reported with UV-A and UV-B irradiation [40,41]. However, the authors failed to find literature confirming their generation by UV-C. Both CPDs and 6-4PPs represent irreversible covalent bonds that critically hinder onsite genomic replication and transcription. Moreover, these lesions cause structural distortion of the genomic material, which may also prevent the optimal replication and transcription in neighboring regions. Cumulatively, these damages generate defects and mutations that frequently result in non-viable microorganisms [35].

Interestingly, pyrimidines have a higher propensity to absorb UV-C photons than purines; thus, pyrimidine-derived photoproducts have a critical role in UV-C activity [42–44]. Nevertheless, the direct antimicrobial activity of UV-C is comprehensively multifactorial, in that it encompasses the metabolic activity, gene expression level (namely mRNA concentration), and existing protective mechanisms of each microorganism. UV-C irradiation in low-pressure mercury lamps has the potential to generate R◎ S, namely ozone (◎ 3) [45]. During ◎ 3 decay, it may generate other R◎ S such as hydroxyl radicals (H◎ •) [46–49]. These R◎ S, in particular H◎ •, are extremely reactive and known to damage proteins, lipids, and nucleic acids [50–53]. The conjugation of these activities may be responsible for lethal genomic mutations, higher cell membrane permeability,

unregulated ion flow, and the loss of cell membrane polarization [54]. The UV-C susceptibility observed among microorganisms, species, and strains has been attributed to several factors, such as cell wall thickness; cell size; pigmentation; the composition, size, conformation, and pyrimidine content of the genetic material; and repair mechanism efficiency [54,55]. Therefore, studies have shown mixed results when evaluating the effectiveness of UV-C light against different microorganisms [35]. It has been described that Gram-positive bacteria are more resistant to UV-C light than Gram-negative bacteria when they are tested under the same conditions [56]. The current study denoted that *S. aureus* ATCC 6538 (Gram-positive) displayed a higher resistance to UV-C irradiance compared to *E. coli* ATCC 8739 (Gram-negative). It has been suggested that the extent of UV-C-induced DNA damage in Gram-positive bacteria is lower due to their thicker peptidoglycan walls and higher DNA repair efficacy [57]. Gram-positive bacteria possess cell walls with an average thickness of 30 to 80 nm, while Gram-negative bacteria have a thickness between 2 and 15 nm [58,59]. However, this study denoted a higher susceptibility in *S. epidermidis*, a Gram-positive bacterium. In fact, *S. epidermidis* showed the highest inactivation rate (4.2 $J^{-1}.cm^{-3}$) among all the tested microorganisms. This result underscores the intrinsic differences in the microorganisms. Yeasts were less susceptible to UV-C. This higher resistance has been attributed to several factors: cell size (decreased probability of photons hitting critical structures), the nuclear membrane, and higher levels of repair mechanisms [60].

3.2. UV-C Viability Reduction Efficacy for Ti and PEEK

The absorption and reflectance spectra of Ti and PEEK are depicted in Figure 5.

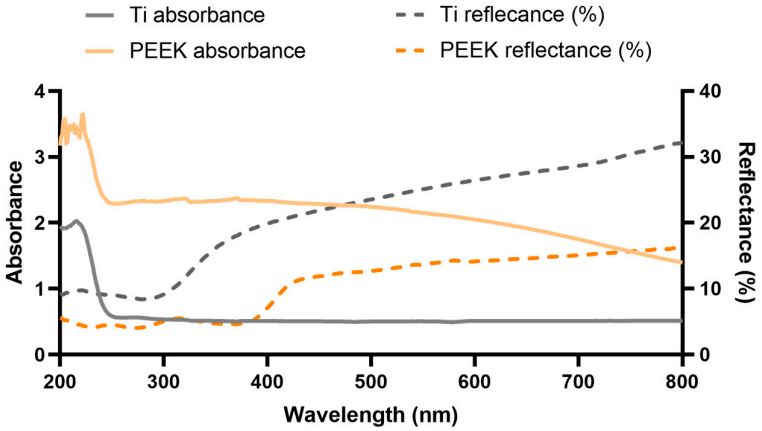

Figure 5. Ti and PEEK absorbance and reflectance spectra.

It should be noted that UV-C has a very low penetration depth, of solely approximately 2 μm [61].

The absorption of TI and PEEK was unexpectedly higher in the visible region, in comparison to GLS, due to their opacity. The absorbance starts to rise further in Ti at 249 nm and reaches its maximum at 216 nm. Nevertheless, it exhibited lower absorption levels then GLS. PEEK's absorbance starts to increase at 241 nm and spikes at 205 nm. It exhibits an absorbance level similar to that of GLS. The reflectance of Ti, which is nearly 32% for the highest wavelength tested, consistently decreases and further drops at nearly 350 nm, stabilizing at approximately 300 nm. PEEK's reflectance, which was nearly two-fold lower than that of Ti at the highest wavelength, also consistently slightly decreased until approximately 425 nm. At lower wavelengths, PEEK's reflectance lowers more rapidly, by nearly 5% from 385 nm to 200 nm. The discrepancy between the absorption and reflectance profiles may highlight the higher scattering in Ti in comparison to GLS. Therefore, Ti may

effectively scatter light until the UV-C region, where this irradiation is able to excite electrons from the valence band into the conduction band, leading to its absorbance [62,63]. Nevertheless, the absorbance range for UV-C light seems to represent a slightly lower wavelength than the 254 nm provided by the low-pressure mercury lamp used. Thus, based on these results, the UV-C absorbance by Ti may not be directly correlated with microorganisms' loss of viability. Nevertheless, transmittance spectra that exhibit nearly full absorption of UV light below around 380 nm may be found in the literature [64]. These differences may be based on the different surface treatments applied to Ti. PEEK is described to nearly absorb the irradiation entirely between 300 and 380 nm [65]. This is corroborated by the reflectance profile. However, the absorbance profile does not display the same tendency as described in the literature, which is inversely proportional to the observed reflectance curve [65,66]. This may be due the very high absorbance values throughout the entire UV–visible light spectra, which may result in the higher temperature variation.

GLS was used as a standard surface; however, all the tested microorganisms displayed a distinct profile when inoculated into the different Ti and PEEK samples. *E. coli* ATCC 25922, *P. aeruginosa*, *C. albicans*, and *C. glabrata* were the representative microorganisms tested on these materials (Figure 6 and Table 3). *P. aeruginosa*, responsible for most implant-related infections, showed a high sensitivity to UV-C radiation on GLS. Interestingly, the UV-C exhibited a loss of effectiveness towards *P. aeruginosa* inoculated into PEEK similar to that observed in *E. coli* (nearly 12-fold). However, the loss rate was clearly higher in Ti, reaching a value nearly 40-fold higher than that observed in GLS. ◎ n titanium surfaces, *E. coli* ATCC 25922 was reduced by 3.7 and 5.2 log CFU.mL^{-1}, respectively, when treated with UV-C light at 19.35 J.cm^{-2} and 38.34 J.cm^{-2}. For PEEK, the reduction in *E. coli* ATCC 25922 was higher, with 2.0 log CFU.mL^{-1} achieved after UV-C treatment at 38.34 J.cm^{-2} (30 s). Similarly, a higher reduction in *E. coli* ATCC 25922 was observed on glass (approximately 7.0 log CFU.mL^{-1} at 6.31 J.cm^{-2}) surfaces compared to titanium and PEEK surfaces. The inactivation rates were higher for less hydrophobic materials with smoother surfaces (GLS and PEEK) as compared to materials with rougher surfaces (Ti). These findings indicate that UV-C light can effectively reduce the tested *P. aeruginosa* and *E. coli* populations on biomaterial surfaces. The log reduction in glass for C. albicans was significantly lower than on the other surfaces, and the loss rate was lower in GLS, reaching a value nearly 2-fold lower than those observed in Ti and PEEK.

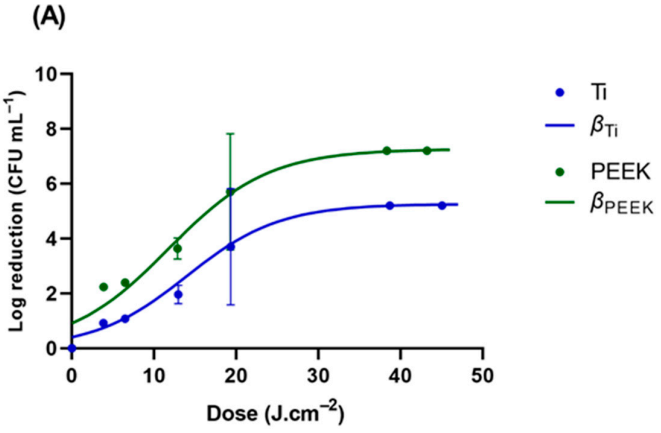

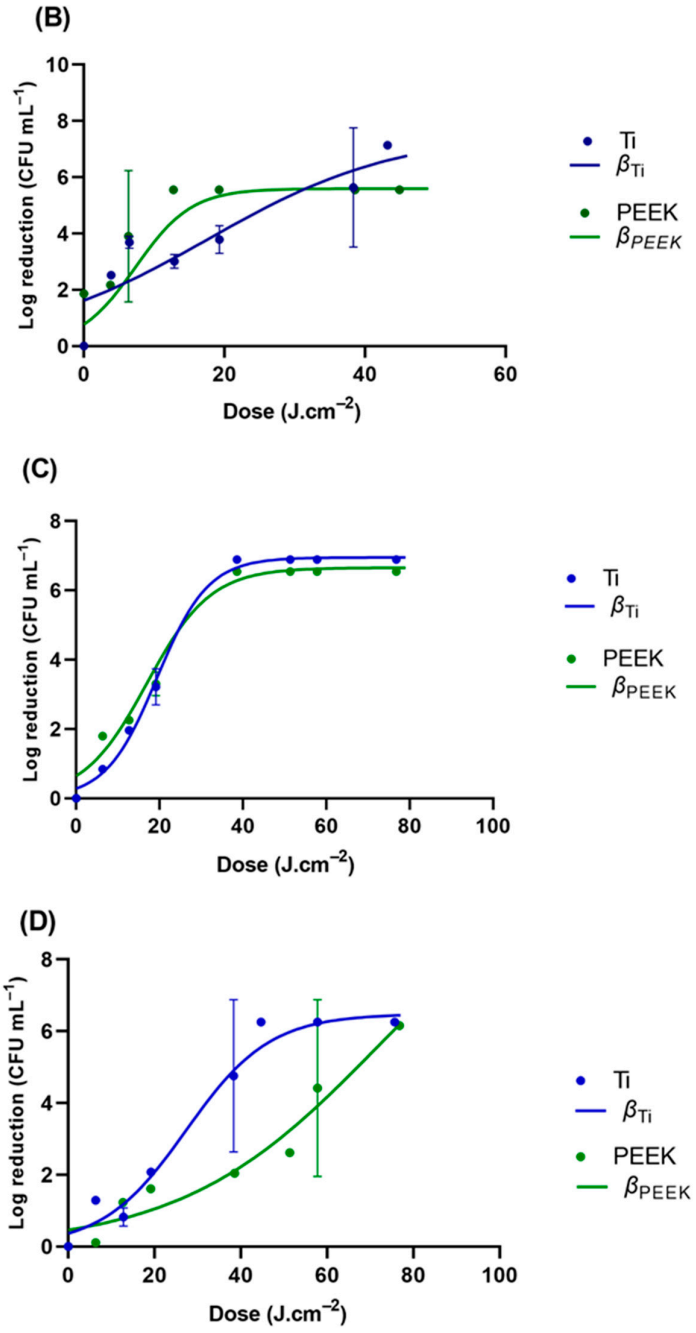

Figure 6. Viability reduction profiles of (**A**) *E. coli strains* ATCC 25922, (**B**) *P. aeruginosa* ATCC 27853, (**C**) *C. albicans* ATCC 10231, and (**D**) *C. glabrata* ATCC 2001 on GLS, TI, and PEEK. β represents the modeled reduction using the logistic equation (Equation (3)).

Table 3. Microorganism models of inhibition according to UV-C irradiation.

Microorganisms	ATCC Strain	Material	R_{max} (CFU.mL^{-1})	R_{min} (CFU.mL^{-1})	μ (J^{-1}.cm^{-3})	Model	r^2
E. coli	25922	Ti	5.26	0.34	0.18	Logistic equation	0.9951
		PEEK	7.26	0.91	0.16	Logistic equation	0.9837

P. aeruginosa	27853	Ti	7.60	1.62	0.07	Logistic equation	0.9078
		PEEK	5.60	0.62	0.25	Logistic equation	0.9761
C. albicans	10231	Ti	6.95	0.28	0.16	Logistic equation	0.9983
		PEEK	6.65	0.57	0.13	Logistic equation	0.9911
C. glabrata	2001	Ti	6.46	0.38	0.10	Logistic equation	0.9968
		PEEK	11.21	0.46	0.04	Logistic equation	0.9732

The study showed a strong correlation between surface roughness and the inactivation of pathogenic microorganisms, considering the glass and PEEK surfaces as smooth surfaces and the Ti surface as a microroughened surface. GLS exhibited the lowest height for the bacterial stacking structure from the basis line, while Ti had the greatest height. The relationship between the roughness values of material surfaces and their bactericidal effect is a topic of debate [47,67–69]. Some researchers have reported that surfaces with lower roughness values tend to be more hygienic [67,68]. UV-C reduced the percentage of pathogenic microorganisms on the treated surfaces compared to non-irradiated surfaces at almost every incubation time. The *E. coli* ATCC 25922, *P. aeruginosa*, and *C. glabrata* inactivation levels differed according to the material surfaces; the bactericidal effect gradually increased in the order of Ti, PEEK, and glass. The UV-C treatment was more effective on the smooth glass surfaces, possibly due to the lack of a protective blasted topography, making it less amenable for *E. coli* cells to attach. It is well established that bacteria on rough surfaces of Ti are shielded by micro-complex construction during treatment [70–72]. The correlation between early bacterial adhesion and surface roughness remains unclear [25,73]. The topography of a material surface can considerably impact the formation of biofilms; however, this is not very relevant to the work since the contact time between the microorganisms and the material surface was rather short. Micro-roughened surfaces are known to have a high susceptibility to bacterial contamination due to their propensity to trap bacteria in micro-pits, which may protect them from UV-C light [73–75]. Surface roughness not only increases the surface area for bacterial adhesion but is also thought to provide a scaffold that facilitates bacterial growth. When examining all the microorganisms, *S. epidermidis* exhibited the highest sensitivity to UV-C radiation. On the other hand, *C. albicans* was found to be highly resistant to UV-C radiation.

4. Conclusions

Surface topography has a complex influence on the efficacy of UV-C treatment for surface microbial reduction. A high degree of surface roughness creates larger shadow pockets or areas, where the microorganisms are not affected by UV-C irradiation. However, it can also allow a relatively uniform two-dimensional distribution of cells on the treated surface, which favors treatment uniformity. On the other hand, a smooth surface does not necessarily guarantee high microbial inactivation by UV-C treatment if the surface is highly hydrophobic, leading to cell clustering. The interaction between light and the substrate, such as light reflection and absorption, also plays a role in the inactivation process. Overall, the fact that a significant level of microbial reduction can be achieved after a very short treatment time shows great promise for using UV-C as a rapid and relatively inexpensive method for reducing the microbial load on a range of different surfaces in medical implant processing. The short UV-C exposure did not considerably increase the tested material temperature; nevertheless, this factor should not be

disregarded. Finally, the precise development of viability reduction models for a preselected range of microorganisms will be useful to safely tailor the UV-C dosage treatment to a specific implant, with minimal impact on the material.

Supplementary Materials: The following supporting information can be downloaded at: https://www.mdpi.com/article/10.3390/microbiolres15030080/s1, Table S1: Temperature variation during UV-C exposure estimated linear equations; Table S2. The results analyzed according to exponential equation; Table S3: The results analyzed according to Monod equation; Table S4. The results analyzed according to Michaelis-Menten equation.

Author Contributions: Conceptualization, J.P.; methodology, A.C. and J.P.; validation, J.P., A.Z., and S.H.; formal analysis, J.P.; investigation, A.C., T.N., and N.S.; resources, Ó.C. and A.Z.; data curation, J.P.; writing—original draft preparation, A.C. and J.P.; writing—review and editing, T.N., N.S., Ó.C., A.Z., and S.H.; supervision, A.Z., S.H., and J.P.; project administration, J.P.; funding acquisition, A.Z. All authors have read and agreed to the published version of the manuscript.

Funding: This work was funded by the European Regional Development Fund through the ⊚ perational Competitiveness Program and the National Foundation for Science and Technology of Portugal (FCT) under the projects UID/CTM/00264/2020 of the Centre for Textile Science and Technology (2C2T) and its base (https://doi.org/10.54499/UIDB/00264/2020, accessed on 1 May 2024) and programmatic (https://doi.org/10.54499/UIDP/00264/2020) components. T.N. acknowledges her PhD Scholarship from FCT (Reference 2022.15386.BD).

Institutional Review Board Statement: Not applicable.

Informed Consent Statement: Not applicable.

Data Availability Statement: The data presented in this study are available on request.

Conflicts of Interest: The authors declare no conflicts of interest.

References

1. Hu, Y.; Li, S.; Dong, H.; Weng, L.; Yuwen, L.; Xie, Y.; Yang, J.; Shao, J.; Song, X.; Yang, D.; et al. Environment-Responsive Therapeutic Platforms for the Treatment of Implant Infection. *Adv. Healthc. Mater.* **2023**, *12*, 2300985. https://doi.org/10.1002/adhm.202300985.
2. Baldin, E.K.; de Castro, V.V.; Santos, P.B.; Aguzzoli, C.; Bernardi, F.; Medeiros, T.; Maurmann, N.; Pranke, P.; Frassini, R.; Roesh, M.E.; et al. Copper incorporation by low-energy ion implantation in PE⊚ -coated additively manufactured Ti6Al4V ELI: Surface microstructure, cytotoxicity and antibacterial behavior. *J. Alloys Compd.* **2023**, *940*, 168735. https://doi.org/10.1016/j.jallcom.2023.168735.
3. Ferraris, S.; Spriano, S. Antibacterial titanium surfaces for medical implants. *Mater. Sci. Eng. C* **2016**, *61*, 965–978. https://doi.org/10.1016/j.msec.2015.12.062.
4. Tobin, E.J. Recent coating developments for combination devices in orthopedic and dental applications: A literature review. *Adv. Drug Deliv. Rev.* **2017**, *112*, 88–100. https://doi.org/10.1016/j.addr.2017.01.007.
5. Munteanu, I.; Turcan, M.; Starodub, E.; Bazgan, S.; Nistreanu, A.; Paslari, T.; Enaki, N.A. Ultraviolet C Radiation for Disinfection and Protection Using Periodical ⊚ ptical Structure for Dental Implant. In Proceedings of the 2022 E-Health and Bioengineering Conference (EHB), Iasi, Romania, 17–18 November 2022; pp. 1–4.
6. Rebelo, R.; Padrão, J.; Fernandes, M.M.; Carvalho, S.; Henriques, M.; Zille, A.; Fangueiro, R. Aging Effect on Functionalized Silver-Based Nanocoating Braided Coronary Stents. *Coatings* **2020**, *10*, 1234.
7. Montanaro, L.; Speziale, P.; Campoccia, D.; Ravaioli, S.; Cangini, I.; Pietrocola, G.; Giannini, S.; Arciola, C.R. Scenery of Staphylococcus implant infections in orthopedics. *Future Microbiol.* **2011**, *6*, 1329–1349. https://doi.org/10.2217/fmb.11.117.
8. Shahi, S.; Khorvash, R.; Goli, M.; Ranjbaran, S.M.; Najarian, A.; Mohammadi Nafchi, A. Review of proposed different irradiation methods to inactivate food-processing viruses and microorganisms. *Food Sci. Nutr.* **2021**, *9*, 5883–5896. https://doi.org/10.1002/fsn3.2539.
9. Romanò, C.L.; Scarponi, S.; Gallazzi, E.; Romanò, D.; Drago, L. Antibacterial coating of implants in orthopaedics and trauma: A classification proposal in an evolving panorama. *J. Orthop. Surg. Res.* **2015**, *10*, 157. https://doi.org/10.1186/s13018-015-0294-5.
10. Lorenzetti, M.; Dogša, I.; Stošicki, T.; Stopar, D.; Kalin, M.; Kobe, S.; Novak, S. The Influence of Surface Modification on Bacterial Adhesion to Titanium-Based Substrates. *ACS Appl. Mater. Interfaces* **2015**, *7*, 1644–1651. https://doi.org/10.1021/am507148n.
11. Pietrocola, G.; Campoccia, D.; Motta, C.; Montanaro, L.; Arciola, C.R.; Speziale, P. Colonization and Infection of Indwelling Medical Devices by *Staphylococcus aureus* with an Emphasis on ⊚ rthopedic Implants. *Int. J. Mol. Sci.* **2022**, *23*, 5958. https://doi.org/10.3390/ijms23115958.

12. Bouhrour, N.; Nibbering, P.H.; Bendali, F. Medical Device-Associated Biofilm Infections and Multidrug-Resistant Pathogens. *Pathogens* **2024**, *13*, 393.
13. Gottenbos, B.; Busscher, H.J.; van der Mei, H.C.; Nieuwenhuis, P. Pathogenesis and prevention of biomaterial centered infections. *J. Mater. Sci. Mater. Med.* **2002**, *13*, 717–722. https://doi.org/10.1023/A:1016175502756.
14. Hernandez, J.L.; Woodrow, K.A. Medical Applications of Porous Biomaterials: Features of Porosity and Tissue-Specific Implications for Biocompatibility. *Adv. Healthc. Mater.* **2022**, *11*, 2102087. https://doi.org/10.1002/adhm.202102087.
15. Bianchera, A.; Catanzano, ◎ .; Boateng, J.; Elviri, L. The Place of Biomaterials in Wound Healing. In *Therapeutic Dressings and Wound Healing Applications*; Wiley: Hoboken, NJ, USA, 2020; pp. 337–366.
16. Vallet-Regí, M.; Lozano, D.; González, B.; Izquierdo-Barba, I. Biomaterials against Bone Infection. *Adv. Healthc. Mater.* **2020**, *9*, 2000310. https://doi.org/10.1002/adhm.202000310.
17. Wekwejt, M.; Dziaduszewska, M.; Pałubicka, A. The problem of infections associated with implants—An overview. *Eur. J. Med. Technol.* **2018**, *4*, 19–26.
18. ◎ luwole, ◎ .M. Biofilm: Formation and Natural Products' Approach to Control—A Review. *Afr. J. Infect. Dis.* **2022**, *16*, 59–71. https://doi.org/10.21010/Ajid.v16i2S.7.
19. Sahoo, J.; Sarkhel, S.; Mukherjee, N.; Jaiswal, A. Nanomaterial-Based Antimicrobial Coating for Biomedical Implants: New Age Solution for Biofilm-Associated Infections. *ACS Omega* **2022**, *7*, 45962–45980. https://doi.org/10.1021/acsomega.2c06211.
20. Su, Y.; Yrastorza, J.T.; Matis, M.; Cusick, J.; Zhao, S.; Wang, G.; Xie, J. Biofilms: Formation, Research Models, Potential Targets, and Methods for Prevention and Treatment. *Adv. Sci.* **2022**, *9*, 2203291. https://doi.org/10.1002/advs.202203291.
21. ◎ liveira, W.F.; Silva, P.M.S.; Silva, R.C.S.; Silva, G.M.M.; Machado, G.; Coelho, L.C.B.B.; Correia, M.T.S. Staphylococcus aureus and Staphylococcus epidermidis infections on implants. *J. Hosp. Infect.* **2018**, *98*, 111–117. https://doi.org/10.1016/j.jhin.2017.11.008.
22. Ploux, L.; Ponche, A.; Anselme, K. Bacteria/Material Interfaces: Role of the Material and Cell Wall Properties. *J. Adhes. Sci. Technol.* **2010**, *24*, 2165–2201. https://doi.org/10.1163/016942410X511079.
23. El-Wassefy, N.; El-Fallal, A.; Taha, M. Effect of different sterilization modes on the surface morphology, ion release, and bone reaction of retrieved micro-implants. *Angle Orthod.* **2015**, *85*, 39–47. https://doi.org/10.2319/012014-56.1.
24. McAllister, D.R.; Joyce, M.J.; Mann, B.J.; Vangsness, C.T., Jr. Allograft update: The current status of tissue regulation, procurement, processing, and sterilization. *Am. J. Sports Med.* **2007**, *35*, 2148–2158. https://doi.org/10.1177/0363546507308936.
25. Han, A.; Tsoi, J.K.H.; Matinlinna, J.P.; Zhang, Y.; Chen, Z. Effects of different sterilization methods on surface characteristics and biofilm formation on zirconia in vitro. *Dent. Mater.* **2018**, *34*, 272–281. https://doi.org/10.1016/j.dental.2017.11.012.
26. Sandri, A.; Tessari, A.; Giannetti, D.; Cetti, A.; Lleo, M.M.; Boschi, F. UV-A Radiation: Safe Human Exposure and Antibacterial Activity. *Int. J. Mol. Sci.* **2023**, *24*, 8331.
27. Raeiszadeh, M.; Taghipour, F. Inactivation of microorganisms by newly emerged microplasma UV lamps. *Chem. Eng. J.* **2021**, *413*, 127490. https://doi.org/10.1016/j.cej.2020.127490.
28. Han, A.; Ding, H.; Tsoi, J.K.H.; Imazato, S.; Matinlinna, J.P.; Chen, Z. Prolonged UV-C Irradiation is a Double-Edged Sword on the Zirconia Surface. *ACS Omega* **2020**, *5*, 5126–5133. https://doi.org/10.1021/acsomega.9b04123.
29. Bak, J.; Ladefoged, S.D.; Tvede, M.; Begovic, T.; Gregersen, A. Dose requirements for UVC disinfection of catheter biofilms. *Biofouling* **2009**, *25*, 289-296. https://doi.org/10.1080/08927010802716623.
30. Beh, C.C.; Farah, S.; Langer, R.; Jaklenec, A. Methods for Sterilization of Biopolymers for Biomedical Applications. In *Antimicrobial Materials for Biomedical Applications*; Domb, A.J., Kunduru, K.R., Farah, S., Eds.; The Royal Society of Chemistry: London, UK, 2019; p. 325-347.
31. Pascoal, S.; ◎ liveira, S.; Monteiro, F.; Padrão, J.; Costa, R.; Zille, A.; Catarino, S.◎ .; Silva, F.S.; Pinho, T.; Carvalho, Ó. Influence of Ultrasound Stimulation on the Viability, Proliferation and Protein Expression of ◎ steoblasts and Periodontal Ligament Fibroblasts. *Biomedicines* **2024**, *12*, 361.
32. Padrão, J.; Nicolau, T.; Felgueiras, H.P.; Calçada, C.; Veiga, M.I.; ◎ sório, N.S.; Martins, M.S.; Dourado, N.; Taveira-Gomes, A.; Ferreira, F.; et al. Development of an Ultraviolet-C Irradiation Room in a Public Portuguese Hospital for Safe Re-Utilization of Personal Protective Respirators. *Int. J. Environ. Res. Public Health* **2022**, *19*, 4854.
33. Schneider, C.A.; Rasband, W.S.; Eliceiri, K.W. NIH Image to ImageJ: 25 years of image analysis. *Nat. Methods* **2012**, *9*, 671–675. https://doi.org/10.1038/nmeth.2089.
34. Vieira, B.; Padrão, J.; Alves, C.; Silva, C.J.; Vilaça, H.; Zille, A. Enhancing Functionalization of Health Care Textiles with Gold Nanoparticle-Loaded Hydroxyapatite Composites. *Nanomaterials* **2023**, *13*, 1752.
35. Nicolau, T.; Gomes Filho, N.; Padrão, J.; Zille, A. A Comprehensive Analysis of the UVC LEDs' Applications and Decontamination Capability. *Materials* **2022**, *15*, 2854.
36. Doremus, R.H. *Glass Science*; Wiley: Hoboken, NJ, USA, 1994.
37. Ravanat, J.-L.; Douki, T.; Cadet, J. Direct and indirect effects of UV radiation on DNA and its components. *J. Photochem. Photobiol. B Biol.* **2001**, *63*, 88–102. https://doi.org/10.1016/S1011-1344(01)00206-8.

38. Huo, H.; He, Y.; Chen, W.; Wu, L.; Yi, X.; Wang, J. Simultaneously monitoring UVC-induced DNA damage and photoenzymatic repair of cyclobutane pyrimidine dimers by electrochemical impedance spectroscopy. *Talanta* **2022**, *239*, 123081. https://doi.org/10.1016/j.talanta.2021.123081.
39. Yokoyama, H.; Mizutani, R. Structural Biology of DNA (6-4) Photoproducts Formed by Ultraviolet Radiation and Interactions with Their Binding Proteins. *Int. J. Mol. Sci.* **2014**, *15*, 20321–20338.
40. Cadet, J.; Douki, T. Formation of UV-induced DNA damage contributing to skin cancer development. *Photochem. Photobiol. Sci.* **2018**, *17*, 1816–1841. https://doi.org/10.1039/C7PP00395A.
41. Bohm, K.A.; Wyrick, J.J. Damage mapping techniques and the light they have shed on canonical and atypical UV photoproducts. *Front. Genet.* **2023**, *13*, 1102593. https://doi.org/10.3389/fgene.2022.1102593.
42. Rastogi, R.P.; Richa; Kumar, A.; Tyagi, M.B.; Sinha, R.P. Molecular Mechanisms of Ultraviolet Radiation-Induced DNA Damage and Repair. *J. Nucleic Acids* **2010**, *2010*, 592980. https://doi.org/10.4061/2010/592980.
43. Sánchez-Navarrete, J.; Ruiz-Pérez, N.J.; Guerra-Trejo, A.; Toscano-Garibay, J.D. Simplified modeling of E. coli mortality after genome damage induced by UV-C light exposure. *Sci. Rep.* **2020**, *10*, 11240. https://doi.org/10.1038/s41598-020-67838-1.
44. Kufner, C.L.; Krebs, S.; Fischaleck, M.; Philippou-Massier, J.; Blum, H.; Bucher, D.B.; Braun, D.; Zinth, W.; Mast, C.B. Sequence dependent UV damage of complete pools of oligonucleotides. *Sci. Rep.* **2023**, *13*, 2638. https://doi.org/10.1038/s41598-023-29833-0.
45. Bosso, A.; Tortora, F.; Culurciello, R.; Di Nardo, I.; Pistorio, V.; Carraturo, F.; Colecchia, A.; Di Girolamo, R.; Cafaro, V.; Notomista, E.; et al. Simultaneous Irradiation with UV-A, -B, and -C Lights Promotes Effective Decontamination of Planktonic and Sessile Bacteria: A Pilot Study. *Int. J. Mol. Sci.* **2023**, *24*, 12951.
46. Claus, H. ◎ zone Generation by Ultraviolet Lamps†. *Photochem. Photobiol.* **2021**, *97*, 471–476. https://doi.org/10.1111/php.13391.
47. Zhang, X.; Yang, C.; Xi, T.; Zhao, J.; Yang, K. Surface Roughness of Cu-Bearing Stainless Steel Affects Its Contact-Killing Efficiency by Mediating the Interfacial Interaction with Bacteria. *ACS Appl. Mater. Interfaces* **2021**, *13*, 2303–2315. https://doi.org/10.1021/acsami.0c19655.
48. Kaushik, N.; Mitra, S.; Baek, E.J.; Nguyen, L.N.; Bhartiya, P.; Kim, J.H.; Choi, E.H.; Kaushik, N.K. The inactivation and destruction of viruses by reactive oxygen species generated through physical and cold atmospheric plasma techniques: Current status and perspectives. *J. Adv. Res.* **2023**, *43*, 59–71. https://doi.org/10.1016/j.jare.2022.03.002.
49. Ghosh, S.; Chen, Y.; Hu, J. Application of UVC and UVC based advanced disinfection technologies for the inactivation of antibiotic resistance genes and elimination of horizontal gene transfer activities: ◎ pportunities and challenges. *Chem. Eng. J.* **2022**, *450*, 138234. https://doi.org/10.1016/j.cej.2022.138234.
50. Seixas, A.F.; Quendera, A.P.; Sousa, J.P.; Silva, A.F.Q.; Arraiano, C.M.; Andrade, J.M. Bacterial Response to ◎ xidative Stress and RNA ◎ xidation. *Front. Genet.* **2021**, *12*, 821535. https://doi.org/10.3389/fgene.2021.821535.
51. Martemucci, G.; Costagliola, C.; Mariano, M.; D'andrea, L.; Napolitano, P.; D'Alessandro, A.G. Free Radical Properties, Source and Targets, Antioxidant Consumption and Health. *Oxygen* **2022**, *2*, 48–78.
52. Sies, H.; Jones, D.P. Reactive oxygen species (R◎ S) as pleiotropic physiological signalling agents. *Nat. Rev. Mol. Cell Biol.* **2020**, *21*, 363–383. https://doi.org/10.1038/s41580-020-0230-3.
53. Juan, C.A.; Pérez de la Lastra, J.M.; Plou, F.J.; Pérez-Lebeña, E. The Chemistry of Reactive ◎ xygen Species (R◎ S) Revisited: ◎ utlining Their Role in Biological Macromolecules (DNA, Lipids and Proteins) and Induced Pathologies. *Int. J. Mol. Sci.* **2021**, *22*, 4642.
54. Urban, L.; Charles, F.; de Miranda, M.R.A.; Aarrouf, J. Understanding the physiological effects of UV-C light and exploiting its agronomic potential before and after harvest. *Plant Physiol. Biochem.* **2016**, *105*, 1–11. https://doi.org/10.1016/j.plaphy.2016.04.004.
55. Baldelli, G.; Aliano, M.P.; Amagliani, G.; Magnani, M.; Brandi, G.; Pennino, C.; Schiavano, G.F. Airborne Microorganism Inactivation by a UV-C LED and Ionizer-Based Continuous Sanitation Air (CSA) System in Train Environments. *Int. J. Environ. Res. Public Health* **2022**, *19*, 1559.
56. ◎ choa-Velasco, C.E.; Ávila-Sosa, R.; Hernández-Carranza, P.; Ruíz-Espinosa, H.; Ruiz-López, I.I.; Guerrero-Beltrán, J.Á. Mathematical Modeling Used to Evaluate the Effect of UV-C Light Treatment on Microorganisms in Liquid Foods. *Food Eng. Rev.* **2020**, *12*, 290–308. https://doi.org/10.1007/s12393-020-09219-y.
57. Kim, H.J.; Yoon, H.W.; Lee, M.A.; Kim, Y.H.; Lee, C.J. Impact of UV-C Irradiation on Bacterial Disinfection in a Drinking Water Purification System. *J. Microbiol. Biotechnol.* **2023**, *33*, 106–113. https://doi.org/10.4014/jmb.2211.11027.
58. Pasquina-Lemonche, L.; Burns, J.; Turner, R.D.; Kumar, S.; Tank, R.; Mullin, N.; Wilson, J.S.; Chakrabarti, B.; Bullough, P.A.; Foster, S.J.; et al. The architecture of the Gram-positive bacterial cell wall. *Nature* **2020**, *582*, 294–297. https://doi.org/10.1038/s41586-020-2236-6.
59. Mai-Prochnow, A.; Clauson, M.; Hong, J.; Murphy, A.B. Gram positive and Gram negative bacteria differ in their sensitivity to cold plasma. *Sci. Rep.* **2016**, *6*, 38610. https://doi.org/10.1038/srep38610.
60. Gabriel, A.A. Inactivation of *Escherichia coli* ◎ 157:H7 and spoilage yeasts in germicidal UV-C-irradiated and heat-treated clear apple juice. *Food Control* **2012**, *25*, 425–432. https://doi.org/10.1016/j.foodcont.2011.11.011.
61. Meinhardt, M.; Krebs, R.; Anders, A.; Heinrich, U.; Tronnier, H. Wavelength-dependent penetration depths of ultraviolet radiation in human skin. *J. Biomed. Opt.* **2008**, *13*, 044030. https://doi.org/10.1117/1.2957970.

62. Lu, S.-y.; Wu, D.; Wang, Q.-l.; Yan, J.; Buekens, A.G.; Cen, K.-f. Photocatalytic decomposition on nano-Ti◎ 2: Destruction of chloroaromatic compounds. *Chemosphere* **2011**, *82*, 1215–1224. https://doi.org/10.1016/j.chemosphere.2010.12.034.
63. Nakhaei, K.; Ishijima, M.; Ikeda, T.; Ghassemi, A.; Saruta, J.; ◎ gawa, T. Ultraviolet Light Treatment of Titanium Enhances Attachment, Adhesion, and Retention of Human ◎ ral Epithelial Cells via Decarbonization. *Materials* **2021**, *14*, 151.
64. Liu, B.; Zhao, X.; Zhao, Q.; He, X.; Feng, J. Effect of heat treatment on the UV–vis–NIR and PL spectra of Ti◎ 2 films. *J. Electron Spectrosc. Relat. Phenom.* **2005**, *148*, 158–163. https://doi.org/10.1016/j.elspec.2005.05.003.
65. Giancaterina, S.; Rossi, A.; Rivaton, A.; Gardette, J.L. Photochemical evolution of poly(ether ether ketone). *Polym. Degrad. Stab.* **2000**, *68*, 133–144. https://doi.org/10.1016/S0141-3910(99)00181-0.
66. Švorčík, V.; Prošková, K.; Rybka, V.; Vacík, J.; Hnatowicz, V.; Kobayashi, Y. Changes of PEEK surface chemistry by ion irradiation. *Mater. Lett.* **1998**, *36*, 128–131. https://doi.org/10.1016/S0167-577X(98)00030-5.
67. Choi, S.H.; Jeong, W.S.; Cha, J.Y.; Lee, J.H.; Lee, K.J.; Yu, H.S.; Choi, E.H.; Kim, K.M.; Hwang, C.J. Effect of the ultraviolet light treatment and storage methods on the biological activity of a titanium implant surface. *Dent. Mater.* **2017**, *33*, 1426–1435. https://doi.org/10.1016/j.dental.2017.09.017.
68. Katara, G.; Hemvani, N.; Chitnis, S.; Chitnis, V.; Chitnis, D.S. Surface disinfection by exposure to germicidal UV light. *Indian J. Med. Microbiol.* **2008**, *26*, 241–242. https://doi.org/10.4103/0255-0857.42034.
69. Mu, M.; Liu, S.; DeFlorio, W.; Hao, L.; Wang, X.; Salazar, K.S.; Taylor, M.; Castillo, A.; Cisneros-Zevallos, L.; ◎ h, J.K.; et al. Influence of Surface Roughness, Nanostructure, and Wetting on Bacterial Adhesion. *Langmuir* **2023**, *39*, 5426–5439. https://doi.org/10.1021/acs.langmuir.3c00091.
70. Bartolomeu, M.; Braz, M.; Costa, P.; Duarte, J.; Pereira, C.; Almeida, A. Evaluation of UV-C Radiation Efficiency in the Decontamination of Inanimate Surfaces and Personal Protective Equipment Contaminated with Phage ϕ6. *Microorganisms* **2022**, *10*, 593.
71. Sousa, V.; Mardas, N.; Spratt, D.; Hassan, I.A.; Walters, N.J.; Beltrán, V.; Donos, N. The Effect of Microcosm Biofilm Decontamination on Surface Topography, Chemistry, and Biocompatibility Dynamics of Implant Titanium Surfaces. *Int. J. Mol. Sci.* **2022**, *23*, 10033.
72. Hirota, M.; Sugita, Y.; Ishijima, M.; Ikeda, T.; Saruta, J.; Maeda, H.; ◎ gawa, T. UV photocatalytic activity of titanium dioxide (Ti◎ 2) surface contaminated with bacterial biofilm: Implications for photo-restoration of osteoconductivity. *Mater. Today Adv.* **2021**, *12*, 100182. https://doi.org/10.1016/j.mtadv.2021.100182.
73. Dantas, T.; Padrão, J.; da Silva, M.R.; Pinto, P.; Madeira, S.; Vaz, P.; Zille, A.; Silva, F. Bacteria co-culture adhesion on different texturized zirconia surfaces. *J. Mech. Behav. Biomed. Mater.* **2021**, *123*, 104786. https://doi.org/10.1016/j.jmbbm.2021.104786.
74. Tardelli, J.D.C.; Bagnato, V.S.; Reis, A.C.d. Bacterial Adhesion Strength on Titanium Surfaces Quantified by Atomic Force Microscopy: A Systematic Review. *Antibiotics* **2023**, *12*, 994.
75. Kowalski, W.; Moeller, R.; Walsh, T.J.; Petraitis, V.; Passman, F.J. Ultraviolet disinfection efficacy test method using bacteria monolayers. *J. Microbiol. Methods* **2022**, *200*, 106541. https://doi.org/10.1016/j.mimet.2022.106541.